

Higgs searches at the Tevatron

Paolo Mastrandrea^a,
on behalf of CDF and DØ collaborations

^aINFN, Sezione di Roma, Piazzale A. Moro 2, 00185 Roma, Italy

Abstract

The search for the Standard Model Higgs boson in $p\bar{p}$ collisions at 1.96 TeV performed by CDF and DØ collaborations at the Tevatron collider is reported in this paper. The Higgs candidate events are reconstructed using different final states in order to optimize the sensitivity in the full range of the Higgs mass. The presented results use different statistical samples collected by the Tevatron up to 5.9 fb^{-1} . Combining the most updated limits provided by the two experiments for all the final states analyzed, the Standard Model Higgs boson is excluded at 95 % C.L. in the mass range 158 - 175 GeV/c², in good agreement with the prediction for the analyzed data sample.

Keywords: Higgs, Tevatron

1. Introduction

The Standard Model of field and particles (SM) [1], [2], [3] is the theory that provides the best description of the known phenomenology of the particle physics up to now. It is a quantum field theory based on the gauge symmetry group $SU(3)_C \times SU(2)_L \times U(1)_Y$, with spontaneous symmetry breaking. This gauge group includes the color symmetry group of the strong interaction, $SU(3)_C$, and the symmetry group of the electroweak interactions, $SU(2)_L \times U(1)_Y$. The formulation of the Standard Model as a gauge theory guarantees its renormalizability, but forbids explicit mass terms for fermions and gauge bosons. The masses of the particles are generated in a gauge-invariant way by the *Higgs Mechanism* [4] via a spontaneous breaking of the electroweak symmetry. This mechanism also implies the presence of a massive scalar particle in the mass spectrum of the theory, the *Higgs boson*. This particle is the only one, among the basic elements for the minimal formulation of the SM, to have not been confirmed by the experiments yet. In the SM, the mass of the Higgs boson is given by $m_H = \sqrt{\lambda/2} \cdot u$, where λ is the Higgs self-coupling parameter and u is the vacuum expectation value of the Higgs field, $u = (\sqrt{2}G_F)^{-1/2} \approx 246 \text{ GeV}/c^2$, fixed by the Fermi coupling G_F , which is determined precisely from muon decay measurements [5]. Since λ is presently unknown,

the value of the m_H can not be predicted. However theoretical arguments [6] can set approximate bounds on the range of possible values for the mass of the SM Higgs boson.

The couplings of the SM Higgs boson to fundamental fermions are proportional to the fermion masses, and the couplings to bosons are proportional to the squares of the boson masses. In particular, the SM Higgs boson is a CP-even scalar, and its couplings to gauge bosons, Higgs bosons and fermions are given by:

$$g_{Hf\bar{f}} = \frac{m_f}{u}, \quad g_{HVV} = \frac{2m_V^2}{u}, \quad g_{HHVV} = \frac{2m_V^2}{u^2},$$

$$g_{HHH} = \frac{3m_H^2}{u}, \quad g_{HHHH} = \frac{3m_H^2}{u^2}$$

where $V = W^\pm$ or Z . In Higgs boson production and decay processes, the dominant mechanisms involve the coupling of the H to the W^\pm , Z and/or the third generation quarks and leptons. The Higgs bosons coupling to gluons, Hgg , is induced at leading order by a one-loop graph in which the H couples to a virtual $t\bar{t}$ pair. Likewise, the Higgs bosons coupling to photons, $H\gamma\gamma$, is also generated via loops, although in this case the one-loop graph with a virtual W^+W^- pair provides the dominant contribution [7].

The cross sections for the production of SM Higgs bosons are summarized in Fig.1 for $p\bar{p}$ collisions at the Tevatron.

The branching ratios for the most relevant decay modes of the SM Higgs boson are shown in Fig.2 as

Email address: paolo.mastrandrea@roma1.infn.it (Paolo Mastrandrea)

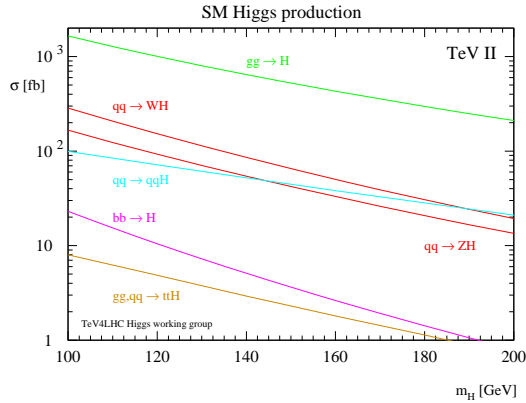


Figure 1: Standard Model Higgs boson production cross section for $p\bar{p}$ collisions at 1.96 TeV.

functions of m_H . For masses below $135 \text{ GeV}/c^2$ (the so-called *low-mass* region), decays to fermion pairs dominate, of which the decay $H \rightarrow b\bar{b}$ has the largest branching ratio. Decays to $\tau^+\tau^-$, $c\bar{c}$ and gluon pairs together contribute less than 15%. For such low masses, the total decay width is less than 10 MeV. For Higgs boson masses above $135 \text{ GeV}/c^2$ (the so-called *high-mass* region), the W^+W^- decay dominates (below the W^+W^- threshold, one of the W bosons is virtual) with an important contribution from $H \rightarrow ZZ$, and the decay width rises rapidly, reaching about $1 \text{ GeV}/c^2$ at $m_H = 200 \text{ GeV}/c^2$ and $100 \text{ GeV}/c^2$ at $m_H = 500 \text{ GeV}/c^2$. Above the $t\bar{t}$ threshold, the branching ratio into top-quark pairs increases rapidly as a function of the Higgs boson mass, reaching a maximum of about 20% at $m_H \sim 450 \text{ GeV}/c^2$.

In the *low-mass* region the process $gg \rightarrow H \rightarrow b\bar{b}$ has the biggest cross section, but is not valuable because of the multijet background, which is overwhelming in an hadronic collider. The associated production of the Higgs boson and a W^\pm or a Z is more rare, but provide a clearer experimental signature. In the *high-mass* region the process $H \rightarrow W^+W^-$ has the biggest branching ratio and provide also a clear signature because of the leptonic decay of the W .

2. Methods

All the presented analysis have been performed utilizing the data collected by the CDF and DØ detectors installed at the Fermilab's Tevatron, an accelerator capable to collide proton with antiproton at a center-of-mass energy $\sqrt{s} = 1.96 \text{ TeV}$ and an instantaneous luminosity $\mathcal{L} = 4 \cdot 10^{32} \text{ cm}^{-2} \text{ s}^{-1}$. Both CDF and DØ are general purpose detectors, cylindrically symmetric around

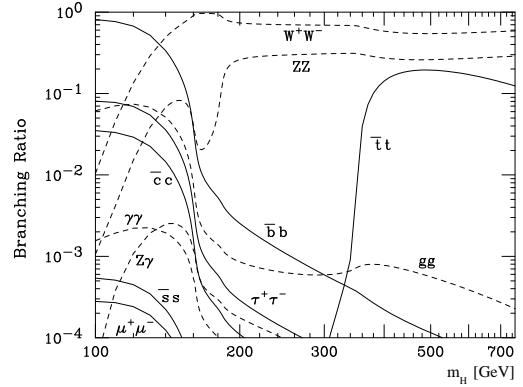


Figure 2: Branching ratios for the Standard Model Higgs boson.

the beam axis which is oriented as the z direction. The polar angle θ is measured from the origin of the coordinate system at the center of the detector with respect to the z axis. The pseudorapidity, transverse energy and transverse momentum are defined as $\eta = -\ln(\tan(\theta/2))$, $E_T = E \sin(\theta)$ and $p_T = p \sin(\theta)$, respectively. Detailed descriptions of the features of the two detectors can be found in [8] and [9].

Several combinations of the W^\pm , Z and Higgs bosons decay channels are utilized to reconstruct the candidate Higgs events. High- p_T electrons and muons are widely used in the reconstruction of the vector bosons candidates because of the clear signatures provided in an hadronic environment. Neutrinos are identified evaluating the missing transverse energy (\cancel{E}_T) in the event. The missing E_T is defined by $\cancel{E}_T = |\vec{\cancel{E}}_T|$, $\vec{\cancel{E}}_T = -\sum_i E_T^i \hat{\mathbf{n}}_i$, where $\hat{\mathbf{n}}_i$ is a unit vector perpendicular to the beam axis and pointing at the i^{th} calorimeter tower. The index i runs over all the calorimeter towers with an energy deposit over a minimum threshold.

The jets are reconstructed using a cone algorithm, with a radius $R = 0.4$. The identification of jets originating from a b -quark (*b-tagging*) is pursued using its long lifetime, high mass and leptonic decay. The main algorithm applied are based on the Reconstruction of a secondary vertex inside the jet cone (*SecVtx*), on the distribution of the tracks inside the jet cone, respect to the primary vertex (*JetProbability*), on the reconstruction of a electron or muon inside the jet cone (*Soft Lepton Tagging*) and on artificial Neural Network.

In order to extract the small signal fraction from the large background in the selected samples, multivariate techniques are widely used. Furthermore, in several channels, the analyzed sample is divided in sub-samples in order to increase the sensitivity.

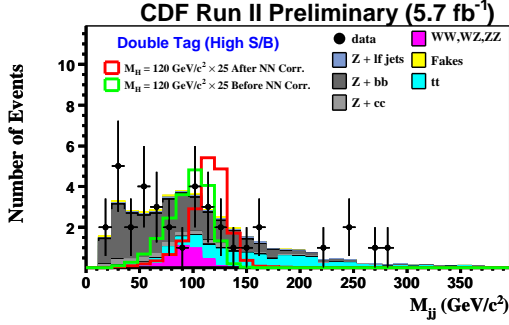


Figure 3: Distribution of the invariant mass of the selected jets, when both are b-tagged, compared with the expected Higgs signal, before and after the correction to the jet energy.

3. Results

The CDF and DØ collaborations are pursuing a direct search for the SM Higgs boson in the $100 < m_H < 200$ GeV/c^2 mass range. In the following the most updated results for the main channels are presented. Only peculiar features will be discussed.

3.1. $ZH \rightarrow l^+l^-b\bar{b}$

The search for events of associated production of an Higgs and a Z boson has been performed by CDF collaboration on a data sample corresponding to 5.7 fb^{-1} . The candidate events are reconstructed using the decays $Z \rightarrow l^+l^-$, where $l = e, \mu$, and $H \rightarrow b\bar{b}$. The $Z \rightarrow l^+l^-$ decays are selected requiring two same-flavor leptons reconstructing to roughly the Z mass ($76 \leq M_{ll} \leq 106 \text{ GeV}/c^2$).

The events selection requires at least two jets within $|\eta| \leq 2$: the first with $E_T \geq 25 \text{ GeV}$ and the second with $E_T \geq 15 \text{ GeV}$.

The selected events are divided into six categories according to the quality of the leptons used to reconstruct

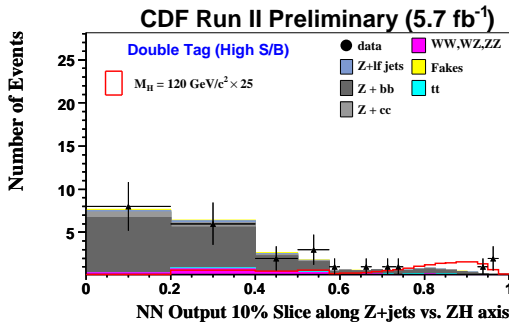


Figure 4: Distribution of the output of the final Neural Network discriminant for the 2 b-tag category.

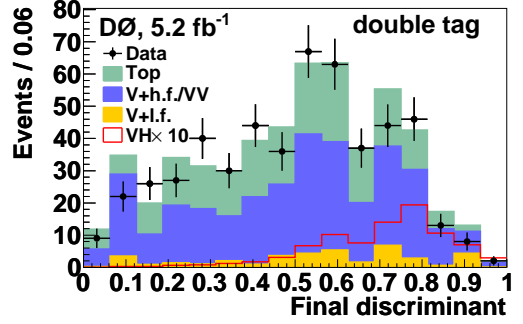


Figure 5: Distribution of the output of the final Neural Network discriminant for the 2 b-tag category for the analysis performed by the DØ collaboration for the $H_T b\bar{b}$ final state.

the Z candidate and to the b-tagging of the jets.

The dijet mass (M_{jj}) is one of the most useful distributions to separate the ZH events the $Z + jets$ background, with its separating power limited mainly by the jet-energy resolution. A Neural Network based technique is used to correct the jet energies, in order to increase the ZH vs $Z + jets$ discrimination.

A final Neural Network based discriminant collects the most powerful kinematic and tagging variable and the Matrix Element probabilities for each event, providing a limit on the ZH production for each category. For a SM Higgs boson mass of $120 \text{ GeV}/c^2$, the expected 95% C.L. upper limit is evaluated to be 6.91 times the SM prediction with an observed limit of 8.32 .

3.2. $ZH \rightarrow \nu b\bar{b}$ and $WH \rightarrow (l)\nu b\bar{b}$

The search for events of low-mass Higgs boson production in the $\cancel{E}_T b\bar{b}$ final state, has been performed by CDF and DØ collaboration on a data sample corresponding to 5.7 fb^{-1} and 5.2 fb^{-1} respectively, with similar techniques. The candidate events are selected requiring large \cancel{E}_T and at least two jets in the region of high efficiency for the b-tagging algorithms. An artificial Neural Network is trained to reduce the multijet background. A final Neural Network based discriminant is used to evaluate the limit on the Higgs boson production.

For a SM Higgs boson mass of $115 \text{ GeV}/c^2$, the 95% C.L. upper limit is observed to be 2.3 times the SM prediction (expected 4.0) by the CDF collaboration, and is observed to be 3.7 times the SM prediction (expected 4.6) by the DØ collaboration.

3.3. $H \rightarrow WW^*$

The search for events of high-mass Higgs boson pro-

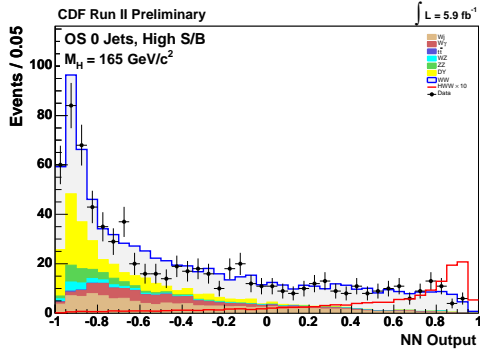


Figure 6: Distribution of the output of the final Neural Network discriminant for the 2 b-tag category for the analysis performed by the CDF collaboration.

duction has been performed by CDF and DØ collaboration on a data sample corresponding to 5.9 fb^{-1} and 5.4 fb^{-1} respectively, using similar techniques. The candidate events are reconstructed using the decays $W \rightarrow l\nu$, where $l = e, \mu$.

The selected events are divided in several categories according to same/opposite sign of leptons, jet multiplicity, selected leptons invariant mass (M_{ll}). Same sign and tri-lepton categories provide acceptance also for the $WH \rightarrow WWW^*$ and $ZH \rightarrow ZWW^*$ channels.

A set of Neural Network based discriminants is used to separate signal from background in the different categories.

For a SM Higgs boson mass of $165 \text{ GeV}/c^2$, the 95% C.L. upper limit is observed to be 1.08 times the SM prediction (expected 1.0) by the CDF collaboration, and is observed to be 1.55 times the SM prediction (expected 1.36) by the DØ collaboration.

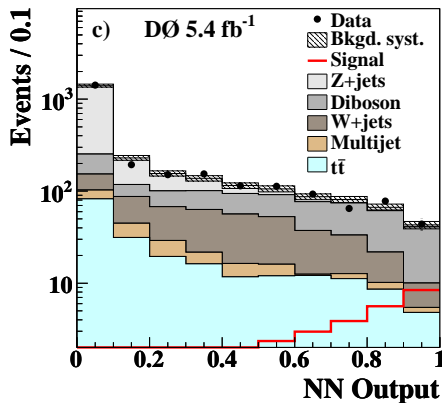


Figure 7: Distribution of the output of the final Neural Network discriminant for the analysis performed by the DØ collaboration. In this case the results for the different categories are combined together in a single discriminant.

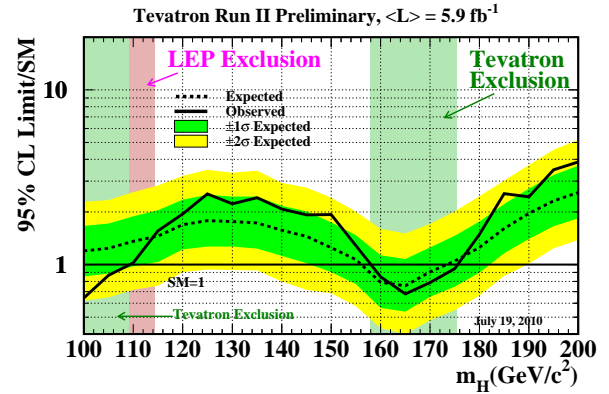


Figure 8: Ratio of the observed 95 % C.L. upper limit to the SM prediction as a function of the Higgs boson mass.

4. Conclusions

All the most updated results for each channel from both the experiments are combined in order to maximize the sensitivity. The statistics and systematics uncertainties are taken into account in the combination procedure, and their correlations are treated consistently. The ratio of the observed 95 % C.L. upper limit to the SM prediction is reported as a function of the Higgs mass in Fig. 8. Tevatron experiments exclude SM Higgs boson at 95 % C.L. for mass between 158 and 175 GeV/c^2 , and between 100 and 109 GeV/c^2 .

References

- [1] S. L. Glashow, *Nucl. Phys.*, 22:579-588, 1961.
- [2] A. Salam, Originally printed in *Svartholm: Elementary Particle Theory, Proceedings Of The Nobel Symposium Held 1968 At Lerum, Sweden*, Stockholm 1968, 367-377.
- [3] S. Weinberg, *Phys. Rev.*, D13:974-996, 1976.
- [4] P. W. Higgs, *Phys. Rev. Lett.* **12**, 132 (1964); *idem*, *Phys. Rev.* **145**, 1156 (1966); F. Englert and R. Brout, *Phys. Rev. Lett.* **13**, 321 (1964); G.S. Guralnik, C.R. Hagen, and T.W. Kibble, *Phys. Rev. Lett.* **13**, 585 (1964).
- [5] T. van Ritbergen and R. G. Stuart, *Phys. Rev. Lett.* **82**, 488 (1999); T. van Ritbergen and R. G. Stuart, *Nucl. Phys.* **B564**, 343 (2000); M. Steinhauser and T. Seidensticker, *Phys. Lett.* **B467**, 271 (1999).
- [6] N. Cabibbo et al., *Nucl. Phys.* **B158**, 295 (1979); See, e.g., G. Altarelli and G. Isidori, *Phys. Lett.* **B337**, 141 (1994); J.A. Casas, J.R. Espinosa, and M. Quirs, *Phys. Lett.* **B342**, 171 (1995); *idem.*, *Phys. Lett.* **B382**, 374 (1996); T. Hambye and K. Riesselmann, *Phys. Rev.* **D55**, 7255 (1997).
- [7] J.F. Gunion et al., *The Higgs Hunter's Guide* (Addison-Wesley) 1990; A. Djouadi, arXiv:hep-ph/0503172 (2005), arXiv:hep-ph/0503173 (2005).
- [8] CDF Collaboration, D.Acosta et al., *Phys. Rev. D* **71** (2005) 032001.
- [9] DØ Collaboration, V. M. Abazov et al, *Nucl. Instrum. Methods Phys. Res., Sect. A* **565**, (2006) 463.